Long-term and regional scale monitoring of CO_2 from space is important for understanding climate changes. Satellite can cover globally but clear sky ratios vary much region by region. Spatial-temporal technique are useful. However, I found several critical issues in this paper. I recommend resubmission.

(1) GOSAT sampling pattern and CO_2 density enhancement over large emission sources; The GOSAT sampling pattern consists of grid observation and target observation. The sampling pattern is not uniform. GOSAT is targeting global megacities which shows local enhancement. Over the ocean, GOSAT is tracking the specular reflection points of the sun, of which sampling pattern is not grid. Authors should describe in more detail how to use these data for analysis.

Dear reviewer, thank you for your kindly suggestions. The characteristics of GOSAT-1/2 data are regional XCO_2 monitoring, and also the function of target observation. Therefore, GOSAT satellite data can be used to calculate carbon emissions from wildfires (Guo M et al., 2017), megacities (Kuze A et al., 2022；Shiomi K et al., 2022), and combined GOSAT-2 and OCO-2 data to calculate terrestrial carbon flux (Wang H et al., 2019). Fig. A1 shows a flowchart of A. Kuze's work (Kuze A et al., 2022；Shiomi K et al.,2022). This work investigates the relationship between the enhancement of near-surface XCO_2 (about 0-4 km) in a time series of dense target observations over megacities and the inverse of the simulated wind speed. This relationship is used to estimate surface CO_2 emissions. The averaged emission intensity for each city was estimated from linear regression slopes in six megacities (Beijing, New Delhi, New York City, Riyadh, Shanghai, and Tokyo). Therefore, the purpose of our work is to fill the data gaps captured by the GOSAT satellite, which may be due to clouds and aerosols, or some locations that cannot be observed by the satellites. With the obtained global high-density coverage data, emission calculations, carbon source and sink, and carbon cycle analysis can be developed more deeply based on GOSAT satellite data (Frankenberg C et al., 2011; Houweling S et al., 2015; Chevallier F et al., 2009; Wang J et al., 2020).
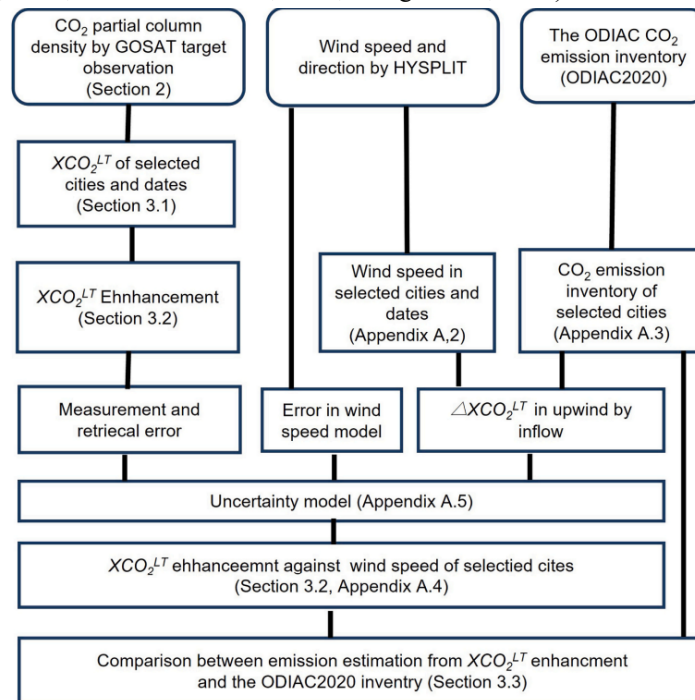
Fig. A1. Flowchart of this study. Critical data are the GOSAT XCO2 LT data products, wind speed from the HYSPLIT transport model, and the ODIAC inventory (Kuze A, 2022)

References:

Guo M, Li J, Xu J, et al. CO2 emissions from the 2010 Russian wildfires using GOSAT data[J]. Environmental pollution, 2017, 226: 60-68.

Kuze A, Nakamura Y, Oda T, et al. Examining partial-column density retrieval of lower-tropospheric CO2 from GOSAT target observations over global megacities[J]. Remote Sensing of Environment, 2022, 273: 112966.

Shiomi K, Kikuchi N, Suto H, et al. Gosat Partial Column Observation for Better Quantifying Urban CO 2 Flux[C]//IGARSS 2022-2022 IEEE International Geoscience and Remote Sensing Symposium. IEEE, 2022: 4350-4352.

Wang H, Jiang F, Wang J, et al. Terrestrial ecosystem carbon flux estimated using GOSAT and OCO-2 XCO$_2$ retrievals[J]. Atmospheric Chemistry and Physics, 2019, 19(18): 12067-12082.

Frankenberg C, Fisher J B, Worden J, et al. New global observations of the terrestrial carbon cycle from GOSAT: Patterns of plant fluorescence with gross primary productivity[J]. Geophysical Research Letters, 2011, 38(17).

Chevallier F, Maksyutov S, Bousquet P, et al. On the accuracy of the CO2 surface fluxes to be estimated from the GOSAT observations[J]. Geophysical Research Letters, 2009, 36(19).

Houweling S, Baker D, Basu S, et al. An intercomparison of inverse models for estimating sources and sinks of CO2 using GOSAT measurements[J]. Journal of Geophysical Research: Atmospheres, 2015, 120(10): 5253-5266.

Wang, J., Feng, L., Palmer, P.I. et al. Large Chinese land carbon sink estimated from atmospheric carbon dioxide data. Nature 586, 720–723 (2020). https://doi.org/10.1038/s41586-020-2849-9

(2) GOSAT data source；I do not understand why authors use the NIES level 3 products. Level 3 products are spatially interpolated already. As mentioned in (1), they are problematic. There are several Level 2 GOSAT products other than NIES such as ACOS, RemoTeC, University of Leicester, and JAXA. Why do authors use NIES products? There is no product defined as "official".

Dear reviewer, thank you for your kindly suggestions. The Level 3 data products are generated from Short Wavelength Infra-Red (SWIR) data observed by Thermal and Near-infrared Sensor for carbon Observation-Fourier Transform Spectrometer (TANSO-FTS) onboard Greenhouse gases Observing Satellite (GOSAT) (hereafter abbreviated as FTS SWIR L3 data products) and that are distributed by the National Institute for Environmental Studies, Japan. The Level 3 products from NIES are downloaded from the GOSAT project data center. And the GOSAT Project is a joint effort promoted by the Japan Aerospace Exploration Agency (JAXA), the National Institute for Environmental Studies (NIES), and the Ministry of the Environment (MOE). Therefore, we consider it to be the official product in the previous manuscript version. But this statement was not rigorous, and we modified the expression that the GOSAT product is the official product in the manuscript. And we added some introduction about GOSAT data, with the addition of " The Level 3 data products are generated from Short Wavelength Infra-Red data observed by Thermal and Near-infrared Sensor for carbon Observation-Fourier Transform Spectrometer (TANSO-FTS) onboard Greenhouse gases Observing Satellite (GOSAT) and that are distributed by the National Institute for Environmental Studies, Japan. The Level 3 products from NIES are downloaded from the GOSAT project data center. And the GOSAT Project is a joint effort promoted by the Japan Aerospace Exploration Agency (JAXA), the National Institute for Environmental Studies (NIES), and the Ministry of the Environment (MOE). "

We are also learning about other GOSAT L2 level products, such as ACOS, RemoTeC, University of Leicester, and JAXA, which are obtained based on the raw data from GOSAT satellite observations through the algorithms of different scientist teams. These works are very well done and have achieved good applications in terrestrial ecological carbon exchange, carbon emission calculation, carbon cycle, carbon sources and sinks (Frankenberg C et al., 2011; Houweling S et al., 2015; Chevallier F et al., 2009; Wang J et al., 2020; Jiang F et al., 2022; Liu J et al., 2014). However, the NIES level 3 products data was selected for several reasons:

1) The Level 3 data is processed based on the Level 2 data. Therefore, the Level 3 data inherits the quality of Level 2 data. And the Level 3 data fills the gaps of Level 2 data on the basis of retaining the quality of Level 2 original data. Besides, benefiting from the format of Level 3 data being fixed point data, the percentage of valid months in the algorithm can be greatly increased during the construction of the parameter library compared to the Level 2 GOSAT products. Within the pre-defined grid, there is a valid cumulative number of months within a year. If the number of valid cumulative months exceeds 10 for the current grid, the data from this grid will be involved in the subsequent construction of the time profile library to obtain a set of time profile parameters. Moreover, the curves that do not satisfy the pattern of CO_2 concentration change curves will be removed from the parameter curve library based on a priori knowledge. Therefore, Level 3 data will be more suitable for our algorithm compared to Level 2 data.

2) The NIES L3 data development and the GOSAT-1/2 satellites that were launched both came from. the Japanese government. Therefore, we concluded that the NIES L3 data would exist a good follow-up data maintenance expected from the Japanese government. Considering the continuous updating and maintenance of our dataset, the NIES L3 data can provide a strong guarantee for continuous updating.

3) The NIES L3 data is extremely easy to find and download from the Japanese GOSAT project data center (https://data2.gosat.nies.go.jp/GosatDataArchiveService/usr/auth/login (last access: 27-October-2022)).

Therefore, for the above reasons, we prefer to select the data from the Japanese GOSAT project data center. Finally, some links are provided to obtain products based on the algorithms of ACOS, RemoTeC, University of Leicester.

1) An XCO_2 dataset developed based on the ACOS algorithm: (https://search.earthdata.nasa.gov/search/granules/collection-details?p=C1633158704-GES_DISC&pg[0][v]=f&pg[0][gsk]=-start_date&q=ACOS_L2S%207.3&tl=1666836734.099!3!!&lat=11.05508932556063&long=59.484375 (last access: 27-October-2022))

2) An XCO_2 dataset developed based on the RemoTeC algorithm: (https://cds.climate.copernicus.eu/cdsapp#!/dataset/satellite-carbon-dioxide?tab=overview (last access: 27-October-2022))

3) An XCO_2 dataset developed from University of Leicester: (https://cds.climate.copernicus.eu/cdsapp#!/dataset/satellite-carbon-dioxide?tab=form (last access: 27-October-2022))

References:

Frankenberg C, Fisher J B, Worden J, et al. New global observations of the terrestrial carbon cycle from GOSAT: Patterns of plant fluorescence with gross primary productivity[J]. Geophysical Research Letters,

2011, 38(17).

Chevallier F, Maksyutov S, Bousquet P, et al. On the accuracy of the CO2 surface fluxes to be estimated from the GOSAT observations[J]. Geophysical Research Letters, 2009, 36(19).

Houweling S, Baker D, Basu S, et al. An intercomparison of inverse models for estimating sources and sinks of CO2 using GOSAT measurements[J]. Journal of Geophysical Research: Atmospheres, 2015, 120(10): 5253-5266.

Wang, J., Feng, L., Palmer, P.I. et al. Large Chinese land carbon sink estimated from atmospheric carbon dioxide data. Nature 586, 720–723 (2020). https://doi.org/10.1038/s41586-020-2849-9

Jiang F, Ju W, He W, et al. A 10-year global monthly averaged terrestrial net ecosystem exchange dataset inferred from the ACOS GOSAT v9 XCO 2 retrievals (GCAS2021) [J]. Earth System Science Data, 2022, 14(7): 3013-3037.

Liu J, Bowman K W, Lee M, et al. Carbon monitoring system flux estimation and attribution: impact of ACOS-GOSAT XCO2 sampling on the inference of terrestrial biospheric sources and sinks[J]. Tellus B: Chemical and Physical Meteorology, 2014, 66(1): 22486.

<Specific Comments>

(1) 2.2 validation data TCCON; When the authors use the muti-year data in TCCON comparison, the coefficient of determination becomes too good. The annual growth of global CO_2 density should be removed for the analysis. The deviation and bias of matched up data should be presented.

Dear reviewer, thank you for your kindly suggestions. This coefficient of determination is obtained by matching the product data to the TCCON value in space and time. Thus, we obtained the coefficient of determination values in Table 1 at each TCCON site. And This coefficient of determination value was obtained normally. However, the evaluation metrics and validation forms of our previous validation experiments were inadequate. Therefore, we supplemented some validation experiments, and the results are shown in Fig. 2.2-1. Besides, the bias ($Bias$) and standard deviation (σ) were added as evaluation indicators in Section 2.4. And the $Bias$ and σ can be calculated as follows:

$$\overline{p} = \frac{1}{N}\sum_{i=1}^{N} P_i, \tag{3}$$

$$Bias = \frac{1}{N}\sum_{i=1}^{N}(P_i - R_i), \tag{5}$$

$$\sigma = \sqrt{\frac{1}{N}\sum_{i=1}^{N}|P_i - \overline{p}|^2}, \tag{6}$$

where N is the number of prediction locations, P_i is the predicted value, and R_i is the observed value.

The Fig. 2.2-1 shows a group diagram about the monthly-averaged XCO_2. The vertical axis of Fig. 2.2-1a is the bias of the calculated monthly-averaged XCO_2 through the TCCON values and the CDC dataset at the mid- and low- latitude stations. Fig.2.2-1b shows the visualized histogram from the data in Fig. 2.2-1a, where the red line in Fig. 2.2-1b is the fitted curve of the Gaussian function. The yellow line is the fitted line. Fig. 2.2-1a show that our bias data are within two standard deviations, and very few points are outside the two standard deviation range. And the mean bias is -0.65pmm for Fig. 2.2-1a. The histogram in Fig. 2.2-1b shows that the bias of the CDC data set with the TCCON data is normally distributed with a mean of -0.63

ppm and a standard deviation of 1.4 ppm. Fig.2.2-1c shows that the R^2 of the CDC data set is 0.97 and the RMSE is 1.38 ppm.
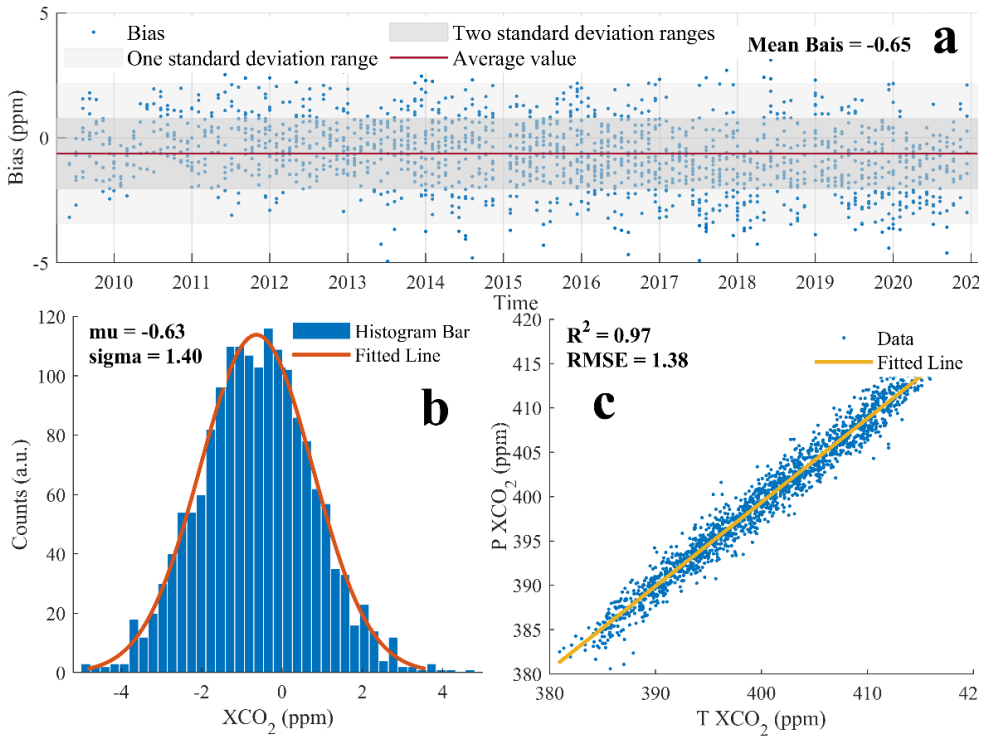

Figure 2.2-1 Monthly-averaged XCO_2 validation results for TCCON data and CDC dataset at global mid- and low-latitude TCCON sites from 200906 to 202012.

For the analysis of interannual XCO_2, we produced scatter error plots for different years at each TCCON site. Moreover, the annual-averaged XCO_2 of TCCON stations and the predicted data annual-averaged XCO_2 in different years are plotted in the station subplots in Fig 2.2-2. And the error bars represent the evaluated RMSE from the TCCON site and the predicted data within different years. Table 2.2-2. represents the annual-averaged errors for different TCCON stations for many years with the inclusion of the indicators R^2 and RMSE. The multi-year XCO_2 evaluation index R^2 is above 0.99 for all 23 sites, with the RMSE evaluation index interval ranging from 0.088 to 0.957 ppm. In particular, the annual-averaged XCO_2 evaluation index R^2 for all sites was 0.999 and the RMSE evaluation index was 0.283 ppm. The deviations and biases of the data matching have been presented and added to Table. 1 in the latest manuscript.

Table 2.2-1. Geographic locations of TCCON sites used for validation and the statistics used to compare predicted annual-averaged XCO_2 and TCCON XCO_2 observations. The " - " represents the number of years for the site is less than 3.

Tccon sites (Site abbreviations)	R^2	RMSE (ppm)
Jet Propulsion Laboratory (JC)	0.988	0.957
Caltech (CI)	0.999	0.232
Edwards (DF)	0.999	0.174

Four Corners (FC)	-	-
Lamont (OC)	0.998	0.356
Park Falls (PA)	0.996	0.568
Manaus (MA)	-	-
Izana (IZ)	0.998	0.387
Ascension Island (AE)	0.986	0.568
Orléans (OR)	0.999	0.329
Zugspitze (ZS)	0.994	0.529
Garmisch (GM)	0.997	0.503
Nicosia (NI)	-	-
Réunion Island (RA)	0.994	0.549
Hefei (HF)	-	-
Burgos (BU)	0.994	0.312
Anmeyondo (AN)	0.999	0.088
Saga (JS)	0.995	0.524
Edwards (DB)	0.997	0.436
Tsukuba (TK)	0.987	0.771
Rikubetsu (RJ)	0.991	0.478
Wollongong (WG)	0.997	0.497
Lauder01&02&03 (LL)	0.996	0.530
AllSites	0.999	0.283

Table 1. Geographic locations of TCCON sites used for validation and the statistics used to compare predicted XCO_2 and TCCON XCO_2 observations.

Tccon sites (Site abbreviations)	Longitude	Latitude	R^2	RMSE (ppm)	Mean Bias(ppm)
Jet Propulsion Laboratory (JC)	-118.18	34.20	0.98**	1.07	-0.89
Caltech (CI)	-118.13	34.14	0.97**	0.95	-1.21
Edwards (DF)	-117.88	34.96	0.98**	0.82	0.72
Four Corners (FC)	-108.48	36.80	0.96**	0.31	-0.75
Lamont (OC)	-97.49	36.60	0.98**	1.04	-1.79
Park Falls (PA)	-90.27	45.94	0.98**	1.24	-0.62
Manaus (MA)	-60.60	-3.21	0.88**	0.64	-1.53
Izana (IZ)	-16.48	28.30	0.98**	1.18	-0.96
Ascension Island (AE)	-14.33	-7.92	0.94**	0.93	-0.84
Orléans (OR)	2.11	47.97	0.99**	0.95	0.13
Zugspitze (ZS)	10.98	47.42	0.92**	1.52	-0.40
Garmisch (GM)	11.06	47.48	0.98**	1.05	0.36
Nicosia (NI)	33.38	35.14	0.93**	0.73	-1.38
Réunion Island (RA)	55.49	-20.90	0.96**	1.23	-1.33
Hefei (HF)	117.17	31.90	0.87**	1.51	-1.82
Burgos (BU)	120.65	18.53	0.89**	1.01	-1.58
Anmeyondo (AN)	120.65	36.54	0.90**	1.20	-0.58

Saga (JS)	130.29	33.24	0.97**	1.26	-1.14
Edwards (DB)	130.89	-12.43	0.99**	0.75	-1.03
Tsukuba (TK)	140.12	36.05	0.91**	1.89	0.48
Rikubetsu (RJ)	143.77	43.46	0.95**	1.17	0.19
Wollongong (WG)	150.88	-34.41	0.99**	0.82	-0.58
Lauder01&02&03 (LL)	169.68	-45.04	0.97**	1.44	-0.70
All sites	-	-	0.97**	1.38	-0.65

** At the 0.01 level (two-tailed), the correlation is significant.
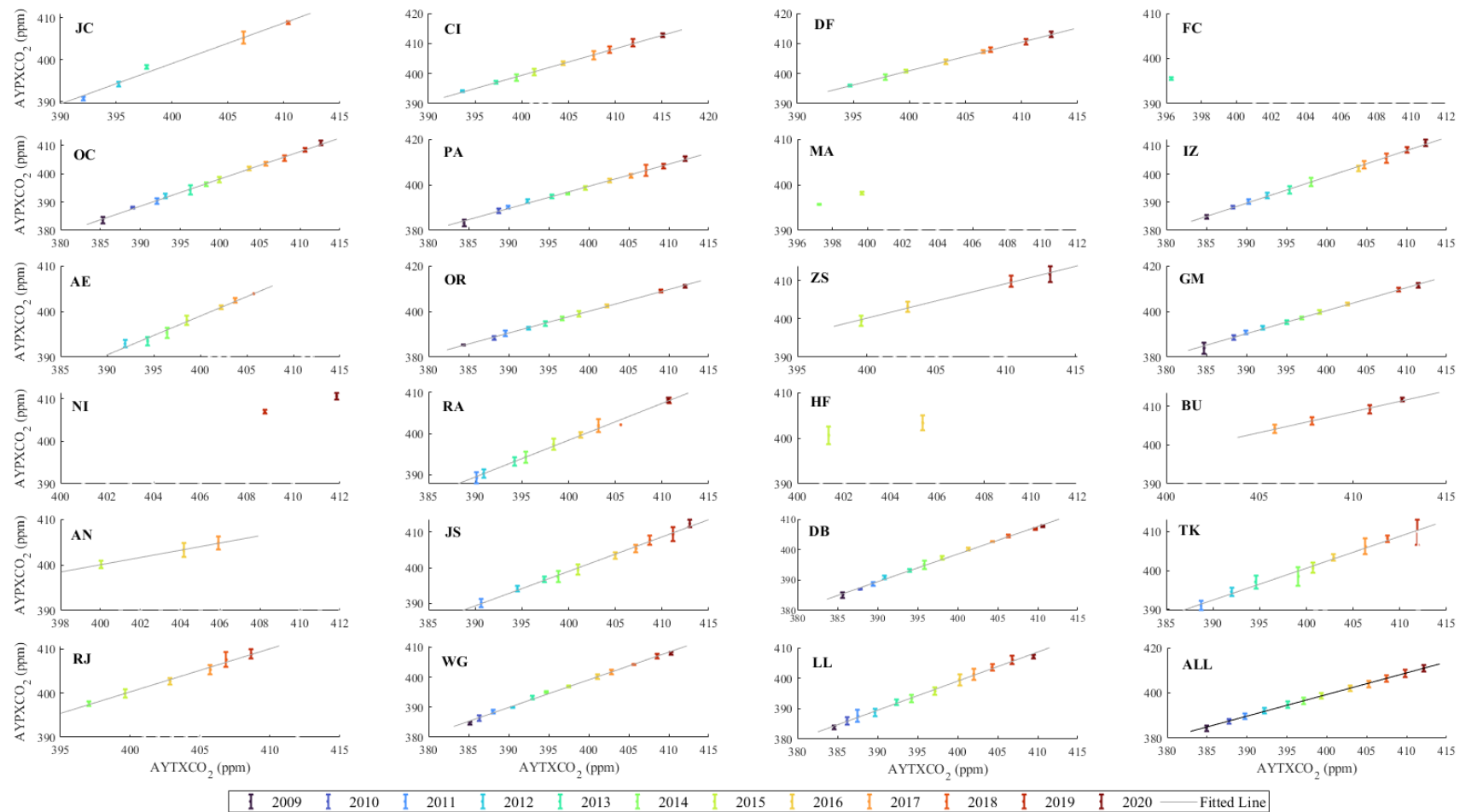
Figure 2.2-2 Scatter error plot of annual-averaged CO_2 concentration. AYPXCO$_2$ represents the predicted annual-averaged CO_2 concentration, AYTXCO$_2$ represents the annual-averaged CO_2 concentration at the TCCON site.

Dear reviewer, thank you for your kindly suggestions. OCO-2_L2_Lite_FP9r (DOI: 10.5067/W8QGIYNKS3JC) is the used version of the OCO-2 data in the previous manuscript. This version has a time interval from 201409 to 202001. However, the National Aeronautics and Space Administration (NASA) team has provided the OCO-2_L2_Lite_FP10r version (DOI: 10.5067/E4E140XDMPO2) now, which mainly addresses the topography-dependent bias as well as the lack of data coverage in 2020.

By update the OCO-2_L2_Lite_FP10r version of the OCO-2 data, this revision reduces the impact of topography-dependent bias in the OCO-2 data and increases the amount of comparative data available in 2020. Therefore, we re-compared the results of the interpolated data with the OCO-2 data in the latest manuscript. The updated results are presented in Figure 4 and Table 2 in the following.
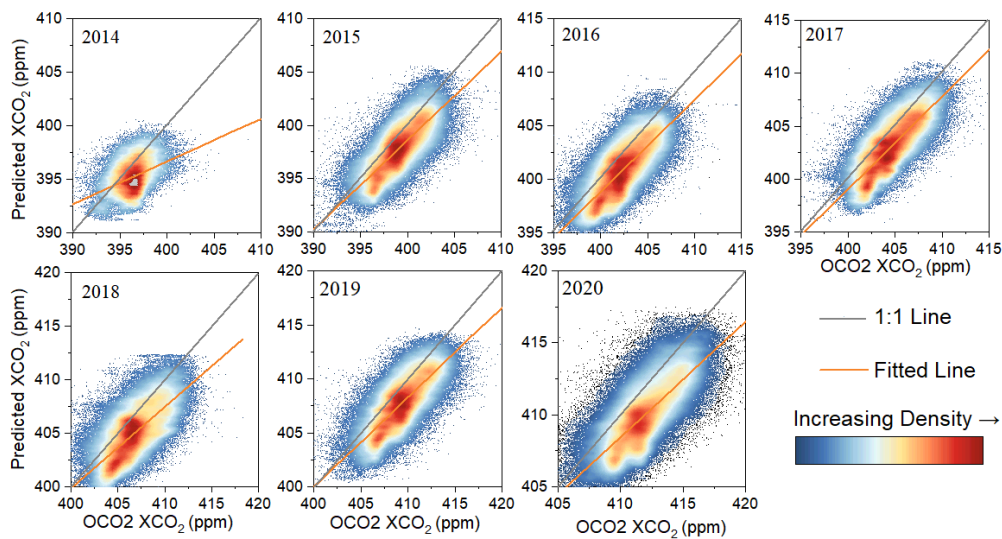
Figure 4. Density scatter plots of predicted XCO_2 and observed one from OCO-2.

Table 2. Statistics for predicted monthly averaged XCO_2 and OCO-2 monthly averaged XCO_2 observations.

Year	R	Nums
2014	0.38**	131463
2015	0.77**	594519
2016	0.76**	791634
2017	0.80**	641891
2018	0.70**	706870

2019	0.76**	785660
2020	0.75**	756116

** At the 0.01 level (two-tailed), the correlation is significant.

Here we provide a description of the CO-2_L2_Lite_FP10r data from the Nasa team.

In early 2021, the OCO Team identified an issue with OCO-2 level 2 products processed since January 28, 2020. The Ancillary Geometric Product (AGAP) file, a static file used in OCO-2 Geolocation processing, was inadvertently replaced with an obsolete version. This AGAP file included a ~300 m pointing error. As a result, all OCO-2 Level 2, version 10r, data files for the period January 28 - December 31, 2020, were corrected and replaced. The replacement process was completed by the end of June, 2021. The significance of this error has been described in Kiel et al. (2019; doi:10.5194/amt-12-2241-2019).

Here, we have provided links to OCO-2 data for both versions.

OCO-2_L2_Lite_FP9r: (https://disc.gsfc.nasa.gov/datasets/OCO2_L2_Lite_FP_9r/summary (last access: 27-October-2022))

OCO-2_L2_Lite_FP10r:(https://search.earthdata.nasa.gov/search/granules/collection-details?p=C1685783927-GES_DISC&pg[0][v]=f&pg[0][gsk]=-start_date&q=OCO2_L2_Lite_FP (last access: 27-October-2022))

B. The difference in footprints of GOSAT and OCO-2 creates errors.

Dear reviewer, thank you for your kindly suggestions. TANSO-FTS-2 is the same as the Fourier Transform spectrometer on the first GOSAT satellite. And the Instant Field of View (IFOV) is 15.8 mrad, which is the same as GOSAT, but the footprint size is smaller - from 10.5 km to 9.7 km - due to the lower altitude of GOSAT-2. Besides, the dimension of 0.25 degree can be used for most requirements. Therefore, we choose 0.25 degree as the size of product data. And Our product data is developed based on mid- and low- latitude grid data. Firstly, the GOSAT data within each grid are averaged, and then subsequent processing is based on the algorithmic framework. Besides, when we did the validation comparison with the OCO-2 data, we directly averaged the OCO-2 data in the corresponding grid, which may contain multiple values of OCO-2. Therefore, the errors caused by the GOSAT data and OCO-2 footprints can be neglected in our paper.

<Technical Corrections>

(1) Page 15 Table 1; Is the unit of RMSE ppm?

Dear reviewer, thank you for your kindly suggestions. The unit of RMSE is ppm, And we have modified the questions you extracted in the latest manuscript. The modified Table 1 is shown in the following.

Table 1. Geographic locations of TCCON sites used for validation and the statistics used to compare predicted XCO_2 and TCCON XCO_2 observations.

Tccon sites (Site abbreviations)	Longitude	Latitude	R^2	RMSE (ppm)	MEAN (ppm)
Jet Propulsion Laboratory (JC)	-118.18	34.20	0.98**	1.07	-0.89
Caltech (CI)	-118.13	34.14	0.97**	0.95	-1.21

Edwards (DF)	-117.88	34.96	0.98**	0.82	0.72
Four Corners (FC)	-108.48	36.80	0.96**	0.31	-0.75
Lamont (OC)	-97.49	36.60	0.98**	1.04	-1.79
Park Falls (PA)	-90.27	45.94	0.98**	1.24	-0.62
Manaus (MA)	-60.60	-3.21	0.88**	0.64	-1.53
Izana (IZ)	-16.48	28.30	0.98**	1.18	-0.96
Ascension Island (AE)	-14.33	-7.92	0.94**	0.93	-0.84
Orléans (OR)	2.11	47.97	0.99**	0.95	0.13
Zugspitze (ZS)	10.98	47.42	0.92**	1.52	-0.40
Garmisch (GM)	11.06	47.48	0.98**	1.05	0.36
Nicosia (NI)	33.38	35.14	0.93**	0.73	-1.38
Réunion Island (RA)	55.49	-20.90	0.96**	1.23	-1.33
Hefei (HF)	117.17	31.90	0.87**	1.51	-1.83
Burgos (BU)	120.65	18.53	0.89**	1.01	-1.58
Anmeyondo (AN)	120.65	36.54	0.90**	1.20	-0.58
Saga (JS)	130.29	33.24	0.97**	1.26	-1.14
Edwards (DB)	130.89	-12.43	0.99**	0.75	-1.03
Tsukuba (TK)	140.12	36.05	0.91**	1.89	0.48
Rikubetsu (RJ)	143.77	43.46	0.95**	1.17	0.19
Wollongong (WG)	150.88	-34.41	0.99**	0.82	-0.58
Lauder01&02&03 (LL)	169.68	-45.04	0.97**	1.44	-0.70
All sites	-	-	0.97**	1.38	-0.64

** At the 0.01 level (two-tailed), the correlation is significant.

(2) page 19, Figure 2; The branching of left and right should be described.

Dear reviewer, thank you for your kindly suggestions. The framework in Figure 2 depicts the general methodology. The workflow of the left branch of Figure 2 is to construct a time-curve parameter library based on the input data, and the workflow of the right branch of Figure 2 is to fill the gaps in the original data on the spatial attributes.

First, section 2.3.2 in the manuscript is visualized in the left branch of Figure2.We pre-divide the grid and then determine whether the input data within each sub-grid is valid input data based on the quality label of the input data. If the cumulative number of valid input data of the grid exceeds 10 in a period (12 consecutive months). Then this grid is a valid month grid and this grid can be used to build the time curve library parameters. The construction of time profile library parameters refers to the extraction of time profile parameters for the valid month grid combined with Equation 1. Finally, the time curve parameters that do not satisfy the requirements are removed based on the a priori knowledge of the CO2 concentration change pattern. And the time profile parameters that meet the requirements are input to the time-profile parameter library.

Second, section 2.3.1 in the manuscript is visualized in the right branch of Figure 2. XCO2 information gaps are filled based on the input data for each month under the perspective of spatial information. Then global mid- and low-latitude projections can be obtained for each month.

Lastly, we incorporated temporal information into the previously acquired surface interpolation data through the proposed transfer component analysis (TCA) theory.
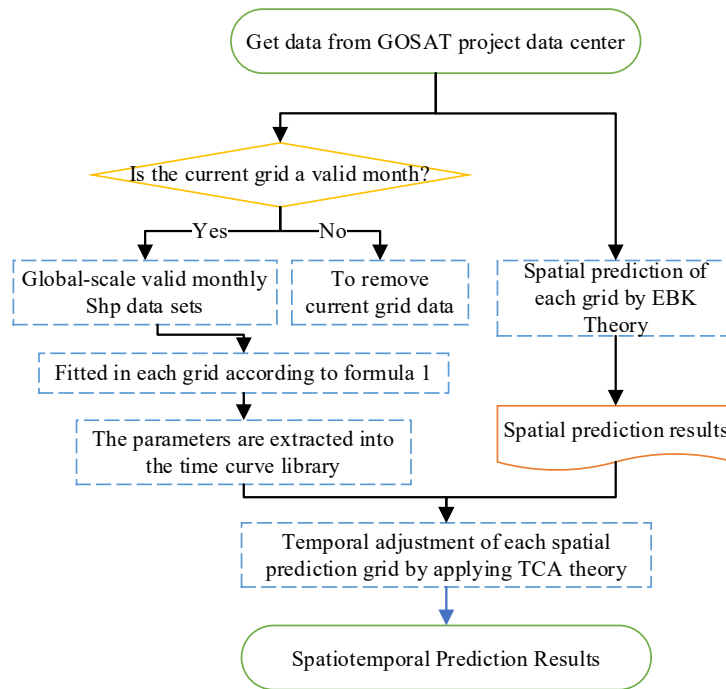
Figure 2. Framework of the proposed methodology